The Role of Slag Carryover on the Non-metallic Inclusion Evolution and Magnetic Behavior in Electrical Steel

ASHOK KAMARAJ, PREMKUMAR MURUGAIYAN, G.K. MANDAL, and G.G. ROY

In the present investigation, a set of high-temperature experimentations were carried out to improve the understanding of the influence of slag carryover (SCO) on non-metallic inclusion evolution during the production of high silicon electrical steels for functional applications. It was observed that the liquid steel treated with synthetic slag and lime resulted in the formation of CaO-based complex oxide, sulfide, and nitride inclusions in the matrix. Whereas the top slag (synthetic slag and lime) contaminated with carryover slag transforms the complex oxide inclusions to Mn free oxy-sulfide inclusions in the high Si steel. Further, the high-silicon steel evaluated for magnetic property confirms the detrimental magnetic behavior of the steel treated using the top slag with the excess amount of SCO (10 kg/t). The increase in coercivity is due to a higher fraction of sub-micron inclusions in the steel matrix. The industry implications of the present findings are highlighted in the light of the evolution of Goss texture in high silicon steel during downstream processing. The evolution of detrimental inclusions in functional grade (electrical) steels due to the presence of SCO call for stringent process control during the upstream processing of liquid steel to maintain the desired magnetic properties.

https://doi.org/10.1007/s11663-022-02547-w

I. INTRODUCTION

THE microstructural sensitive functional properties demand stringent process control of high silicon electrical steel (~3.0 wt pct) compared to other steel grades. It is to be noted that the presence of non-metallic inclusions (NMIs), even in a very small amount within the steel matrix, is sufficient to significantly influence the downstream processing, mechanical, electrical, and magnetic properties of the steel. Several studies[1–6] focused on controlling oxide inclusions during the secondary steelmaking process to improve the magnetic property of the electrical steels. Zinngrebe *et al.*[1] studied the evolution of the inclusion population and reported the dependency of complex assemblages of oxides, sulfides, and nitrides in silicon steel during secondary steelmaking. Kurosaki *et al.*[2] studied the effect of morphology of oxide inclusions on the core loss of semi-finished electrical steel. They reported that elongated oxides reduce the core loss more than spherical oxide inclusions. Petrovic *et al.*[3] stated that Mg vapor released due to alumino-thermic reduction of MgO in refractory assists in generating complex spinel/sulfide/oxy-sulfide inclusions in silicon steel. Luo *et al.*[4] studied MnO concentration in NMIs and its influence on the number density of inclusions in electrical steel. They reported a drastic reduction in the number density of inclusions containing more than 10 wt pct MnO in electrical steels.[4] It is also reported that the inclusion population and density in electrical steel depend more on the concentration of MnO in NMIs than other factors such as cooling rate, superheat, and refractory composition. Shinkagi *et al.*[5] stated that core loss could be reduced by controlling the number density of 1-3 μm size Ca and/or Mg-based oxide inclusions. To improve the magnetic property in electrical steel, Lin *et al.*[6] investigated the effect of deoxidation practice during the RH process to eliminate the complex discretized type inclusions in electrical steel.

ASHOK KAMARAJ is with the Academy of Scientific and Innovative Research (AcSIR), Ghaziabad 201002, India and with the Department of Materials Science and Metallurgical Engineering, Indian Institute of Technology Hyderabad, Kandi, Sangareddy 502285, India and also with the CSIR-National Metallurgical Laboratory (CSIR-NML), Jamshedpur 831007, India. Contact e-mails: srhsbioboy@yahoo.co.in; ashokk@msme.iith.ac.in PREMKUMAR MURUGAIYAN and G.K. MANDAL are with the Academy of Scientific and Innovative Research (AcSIR) and also with the CSIR-National Metallurgical Laboratory (CSIR-NML). G.G. ROY is with the Academy of Scientific and Innovative Research (AcSIR) and also with the Indian Institute of Technology (IIT), Kharagpur 721302, India.

Manuscript submitted October 29, 2021; accepted April 29, 2022.
Article published online May 12, 2022.

The influence of soft killing practice on the desulfurization of ultra-low carbon electrical steel was studied by He *et al.*[7] It is reported that optimizing slag composition by adding synthetic slag during the RH process to control the oxygen potential results in efficient desulfurization of liquid steel. A few published reports suggested that the precipitation and distribution of sulfide inclusions within the steel matrix can be controlled by engineering the oxide inclusions.[6,8] The theoretical investigation of Liu *et al.*[8] highlighted the formation of sulfide precipitates on oxide inclusions in Fe-3 wt pct Si alloys. They concluded that solubility and precipitation of MnS from oxide inclusions could be controlled by the sulfide capacity and extent of MnO concentration in the oxide inclusions. It is also reported that trace elements like sulfur, nitrogen, and carbon should be carefully controlled in electrical steel to avoid deleterious precipitation in a size range of 10-400 nm with smaller inter-particle distance. Kaliz *et al.*[9] and Podorska *et al.*[10] investigated the effect of non-uniform distribution of NMIs in electrical steel and mentioned that deoxidation practice plays a vital role in controlling the interfacial energy of inclusions and liquid steel during solidification. It is also noted that the addition of cerium as a deoxidizer controls the sulfide inclusions and improves the magnetic property in electrical steel.[11,12]

Many studies systematically identified the inclusion formation sources and their development during the steelmaking process, starting from primary steelmaking to casting[13–16] in structural steels. Investigation about the generation and evolution of inclusions in liquid steel narrows down to the focused analysis of secondary steelmaking practices[4] in recent days. In industrial steelmaking operations, liquid steel invariably contains some carryover slag; its composition and quantity vary from heat to heat. It is well reported that the carryover of oxidizing slag into the transfer ladle alters the top slag composition during the steel refining process and hence limits the extent of desulfurization.[7] However, limited attention has been given to understanding SCO's influence (a sub phenomenon) on inclusion control. Though few reports are available related to the control of oxide, sulfide, and oxy-sulfide inclusions in electrical steel,[3,4] the influence of inclusion evolution in the presence of SCO during the production of high silicon steel is scarcer.

It is well known that the core loss of high-silicon electrical steel could be minimized by maximizing the growth of Goss grain through engineering the sulfide (and/or nitride) inclusions.[17] Several investigators[18–25] studied the role of inclusions/non-magnetic particles on the coercivity of the magnetic materials in detail. Dijkstra *et al.*[18] confirmed the dependency of coercive force on the overall volume fraction of inclusions and their state of dispersion within the steel matrix. It is also reported that the coercive force, in general, is not dependent on particles of size much smaller and much larger than the thickness of the domain wall for any steel composition. Later, English[21] experimented with Neel's theory on the coercive force in ferromagnetic material and reported that extremely small ($< 0.1\ \mu m$) particles will be ineffective to pin the domain walls to increase the coercive force. Further, it is also reported that micron-size particles significantly increase the coercivity but do not follow Neel's mechanism of domain wall pinning. Turner *et al.*[23] studied the role of Mn(Cu)S precipitate on the magnetic properties of grain-oriented steel based on local Barkhausen noise measurements. It is confirmed from the BN measurements that residual fine sulfide inclusions (5-10 nm) do not affect the bulk magnetic properties. However, coarse precipitates (100-125 nm) deteriorate the functional properties. Recently, Liu *et al.*[25] studied the interaction between the grain boundary on precipitate on minor BH loop measurements and reported (i) the complex behavior of magnetic parameters due to the interaction of grain boundaries and sulfide inclusions on domain wall pinning and (ii) the significance of critical size and number density of inclusions on the particular phenomenon.

It should be noted that the know-how to produce high-grade electrical steel is kept secret and available only to a few steel producers. Emerging interest in producing electrical steel in India also necessitates an in-depth understanding of the evolution of NMIs during liquid steel refining and its influence on magnetic behavior. Moreover, a systematic study pertaining to the influence of SCO on the evolution of NMIs in high-Si electrical steel is necessary, keeping in view the requirement for high-grade electrical steel. This investigation focuses on the evolution of NMIs in Al-Si killed 3.0 wt pct silicon steel during top slag treatment using synthetic slag and lime contaminated with/without primary steelmaking carryover slag (0-10 kg/t). Further, a detailed characterization of the NMIs and magnetic properties of steel is carried out to enhance the understanding of the product engineering of high-quality electrical steel.

II. EXPERIMENTAL PROCEDURE

A. *Experiment Procedure*

A set of melting and refining experiments was conducted in a 20 kg induction melting furnace (Make: CONSARC). The furnace crucible with dimensions of about 100 mm inner diameter and 250 mm height was used to study the influence of SCO on NMIs in 3.0 wt pct Si steel. A monolithic basic (MgO-based) lining (~5 mm thickness), akin to industrial practice, was used in the induction furnace crucible. The extra-deep drawable (EDD) grade steel scraps were used as starting material for the melting experiments. Laboratory-grade pure silicon and aluminium with 99.99 wt pct purity were used as deoxidizer/alloying elements. After melting the EDD grade steel scraps (15 kg) in an air induction furnace, a predefined amount of pure Si and Al were added in different stages to prepare the liquid steel bath with 3.0 wt pct silicon. After the first-time addition of deoxidizer, 200 g of synthetic slag ($43CaO\text{-}43Al_2O_3\text{-}6.0SiO_2\text{-}8.0MgO$ (all in wt pct)) and 100 g of laboratory-grade lime powder were added to protect the melt from atmospheric reoxidation. The chemical and thermal homogenization of the liquid metal was ensured by

keeping the liquid bath at the desired temperature for 5 minutes after every addition. The liquid steel sample was collected using a specially designed lollypop sampler (refer Figure 1) to ensure the chemical composition during the alloying period (till it reaches 3.0 wt pct Si, i.e., S-1 to S-4). After achieving 3.0 wt pct silicon in the liquid steel, the slag metal reactions continued for 30 minutes in the induction furnace. The lollypop sample was also collected intermittently every 10 minutes (i.e., S-5 to S-7). For the experiments conducted with a predefined amount of SCO (Heat 1: 0, Heat 2: 5, and Heat 3:10 kg/t of liquid steel), the carryover slag (50CaO-4.5MgO-14.0SiO_2-22.0FeO-1.0 MnO-3.5Al_2O_3-2.0P_2O_5 (all in wt pct)) was added into the bath after the deoxidizer addition (S-1). The range of SCO was decided based on the industry experience and reported information.[26–28] After the complete melting of the carryover slag, the synthetic slag and lime powder were added. The slag thickness above the liquid steel was carefully measured by dipping the tied double wires into the liquid bath, consisting of copper and galvanized (GI) steel. The slag thickness was measured by observing the selective melting of the copper wire and GI wire till the top of the slag layer and slag-metal interface due to the difference in the melting point, respectively. The final slag samples were obtained by dipping a steel rod into the molten slag and subsequently quenching it in water. The slag attached to the rod was collected separately and preserved for chemical analysis. The schematic representation of various stages of the experiment, along with the sampling scheme, is shown in Figure 2. The alloying and refining stages of the experiments are referred to as S-1 to S-4 and S-5 to S-7 in the plots/graphs presented in the next section, respectively.

1. *Sample preparation and chemical analysis*

Chemical analysis of steel samples was carried out using an optical emission spectrometer (OES BRUKER Q8 MAGELLAN). The head portion of the lollypop sample was used for chemical analysis (refer Figure 1).

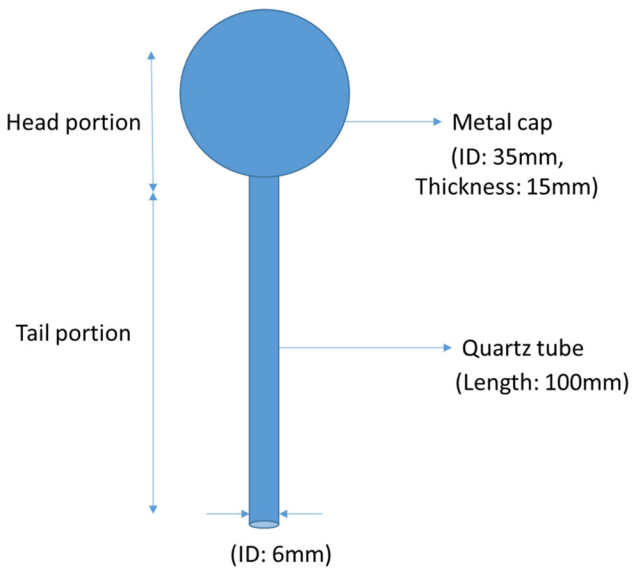

Fig. 1—Schematic of the lollypop sampler used in experiments.

Standard techniques were followed to prepare the steel specimens for chemical analysis. The tail portion of the specially designed lollypop sample was used for total oxygen and nitrogen analysis. The composition of the slag samples was obtained using an X-ray fluorescence (XRF) spectrometer and conventional wet analysis.

2. *Characterization of Non-metallic Inclusions*

The detailed metallographic characterization of NMIs was performed to determine the composition, size, and distribution of inclusions in the steel specimens. Metallography samples were prepared by sectioning the tail portion of the lollypop samples for inclusion analysis. A standard metallography sample preparation technique was followed to prepare the samples. The polished unetched samples, cleaned thoroughly using an ultrasonic cleaner, were used for the NMI characterization using an electron probe microanalyzer (EPMA, Model: JEOLJXA-8230) and automated SEM-EDS (Model: Zeiss SEM EVO18, EDS-OXFORD Instruments). Detailed compositional analysis and elemental mapping were carried out using energy/wavelength dispersive spectroscopy (EDS/WDS, Model: GENESIS) attached with the EPMA. A few selected samples were considered for detailed quantitative characterization of NMIs in the steel matrix using automated SEM-EDS coupled with AZtecsteel software (Make: OXFORD Instruments).

3. *Characterization of magnetic properties*

The steel samples obtained from the steel ingots of Heat 1, 2 and 3 were subjected to magnetometry and fluxmetery techniques to understand the magnetic properties of the sample conditions. The samples obtained from final ingots were hot-rolled at 1100 °C and annealed to remove the microstructural inhomogeneities present in the cast structure. The room temperature saturation magnetization (M–H) curves were obtained from Vibrating Sample Magnetometer (VSM, Model: Versalab, Quantum Design) with a maximum external magnetic field of 1.2 T. A 10 mg of samples were sectioned from the tail portion of the lollypop sample for the VSM study. An in-house developed non-invasive, surface-based magnetic hysteresis loop sensor system, ''MagStar,'' was also employed to understand further the inclusion behavior on the bulk magnetic properties.[29] The bulk magnetic measurements were carried out on four surfaces of parallelepiped samples of 40 mm × 22 mm × 4 mm. Subsequently, macro hardness (Model: 251VRSA Make: AFFRI) and grain size data were obtained from the sample area of interest.

III. RESULTS

A. *Slag Thickness*

Figure 3 represents the slag thickness measured after flux and SCO addition (S-1) and before the occurrence of slag-metal reaction (S-4). The figure clearly shows the increase in slag thickness with SCO. The decrease in slag thickness in stage 4 (S-4) in comparison to stage 1 (S-1) in all the studied Heat is due to the intermediate slag

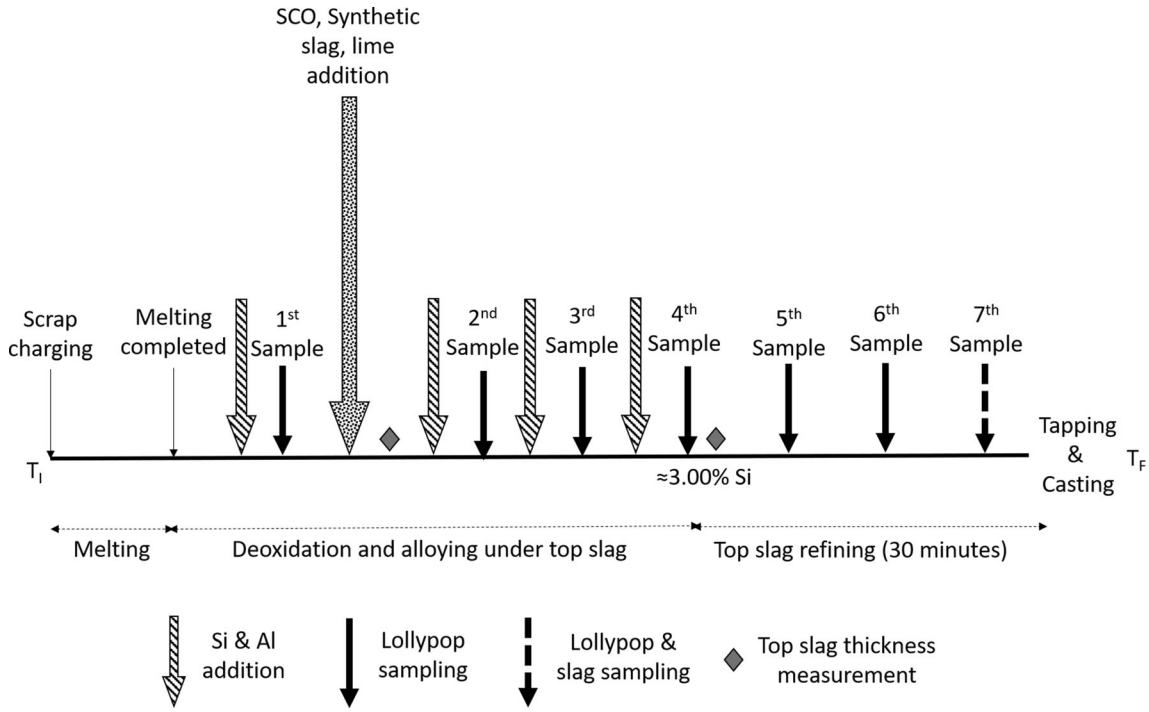

Fig. 2—Schematic representation of various stages of the experiment along with sampling scheme.

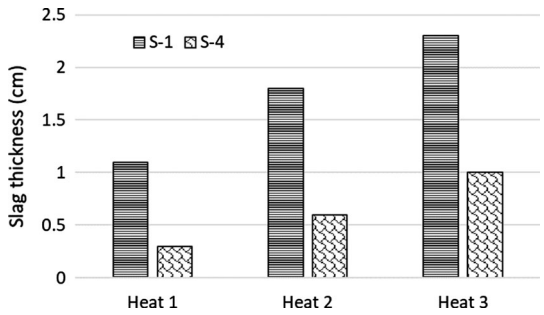

Fig. 3—Measured slag thickness at S-1 and S-4 stages for experiments conducted with different amounts of SCO (Heat 1: 0 kg/t, Heat 2: 5 kg/t, and Heat 3: 10 kg/t).

removal during the liquid steel sampling process. The final slag composition obtained from all three heats is given in Table I. It should be noted that the basicity of final slags varies in a narrow range (0.64-0.71); however, dissolution of MgO from refractory increases with an increase in SCO content in the slag.

1. *Phosphorous reversion and desulfurization*

The detailed chemical analysis of the liquid steel obtained from the specimens of Heat 1, 2, and 3 at different stages of deoxidation, alloying, and refining are given in Table II. The phosphorus content in the liquid steel marginally increases to 86 ppm for the experiment conducted without carryover slag. However, the final phosphorus content of liquid steel increased to 170 ppm and 210 ppm for the Heat with 5 and 10 kg/t SCO, respectively. Similarly, the experiments conducted with various amounts of SCO resulted in poor desulfurization.

2. *Size and distribution of inclusions*

The size and distribution of inclusions within the steel matrix after refining treatment were investigated using the metallographic specimens prepared from the tail portion of the lollypop samples. The quantitative analysis of NMIs present in steel samples was performed, and the results are presented in Figure 4. Figure 4 shows the variation of average size and area fraction NMIs present in the steel samples treated without and with the addition of 5 and 10 kg/t of SCO. The average size of NMIs present in the samples collected at the end of slag-metal refining (S-7) is comparable in all three Heats (with and without the addition of SCO), as depicted in the figure. Figure 4 also reveals the significant increase in the area fraction of NMIs in the Heat 3 sample, obtained after treating with an excess amount of SCO (10 kg/t).

3. *Composition of inclusions*

The morphology and composition of NMIs for the samples collected at the end of the refining period (S-7) for Heat 1, 2, and 3 are examined using SEM/EPMA-EDS. The SEM micrographs represented in Figures 5, 6, and 7 reveal the presence of different types of inclusions in the high silicon electrical steel after top slag refining for Heat 1, 2, and 3, respectively. The generation of deoxidation product (pure SiO_2) and precipitation of MnS in the steel matrix is observed in the Heat 1 steel sample, as shown in Figures 5(a) and (b), respectively. The complex oxide inclusions with globular morphology observed in the Heat 1 sample, as shown in Figures 5(c) and (d), suggest that they are liquid inclusions at steelmaking temperatures. The NMIs observed in the Heat 2 sample are pure MnS

and complex oxide inclusions (with trace MnS in the periphery), as shown in Figures 6(a) and (b), respectively. The NMIs observed in the sample of Heat 3 are co-precipitated nitride-sulfide inclusions and oxy-sulfide inclusions, as shown in Figures 7(a) through (d).

The detailed characterization of the globular complex oxide inclusions was based on elemental mapping using EDS attached with EPMA. Figure 8(a) shows the elemental mapping of the complex oxide inclusions observed in the Heat 1 specimen. The intensity of the MnS ring around the complex oxide inclusion observed in the Heat 2 sample (refer Figure 8(b)) confirms the nature of composite inclusion. Figure 8(c) reveals the sulfur enriched complex oxide inclusion present in Heat 3. Therefore, the transformation of complex oxide inclusion to complex oxide with MnS ring and then to oxy-sulfide inclusion with an increase in the contamination level of carryover slag in the top slag during the preparation of the high silicon steel is confirmed.

A detailed analysis of the complex oxide NMIs in the steel samples was performed using Wavelength Dispersive X-ray Spectroscopy (WDS) attached with the EPMA. The line scan performed across the individual complex oxide NMI, present in the samples of Heat 1, 2, and 3, is represented in Figure 9. It is apparent from Figure 9(a) that the complex oxide inclusions are free from sulfur and manganese in the steel sample treated with only synthetic slag and lime. The analysis also reveals the high concentration of MgO in the middle portion of the oxide inclusion. The complex oxide inclusion observed in the steel sample treated with synthetic slag, lime, and 5 kg/t of SCO is also free from sulfur and manganese, as represented in Figure 9(b). However, the manganese and sulfur peaks appear at the periphery of the oxide inclusion. It may be attributed to the precipitation of the MnS ring around the existing oxide inclusion during the solidification of the high silicon steel. The inclusions present in the Heat conducted with 10 kg/t of SCO are completely different from the other studied Heat and confirmed to be oxy-sulfide inclusions, as confirmed in Figure 9(c). It is

Table I. Chemical Analysis of Final Slag Obtained From Heat 1, 2 and 3

Heat No	CaO	SiO_2	Al_2O_3	MgO	P_2O_5	MnO
1	20.08	28.13	30.77	19.19	0.0021	1.81
2	22.10	34.64	20.55	21.34	0.0069	1.35
3	18.05	26.15	15.53	39.33	0.0572	0.90

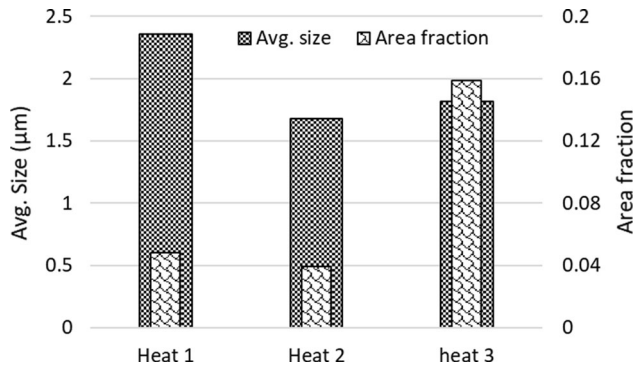

Fig. 4—Quantitative analysis of NMIs in S-7 of all Heats.

Table II. Chemical Analysis of Liquid Steel in Heat 1, Heat 2, and Heat 3

		Deoxidizers Added (g)		Chemical Composition of Liquid Steel (wt pct)					
Sampling Stage	Heat No.	FeSi	Al	Pct C	Pct Si	Pct Al	P (ppm)	S (ppm)	SCO (kg/t)
1	1	70	5.2	0.046	0.216	0.0070	71	48	0
2		147	6.5	0.052	1.227	0.0147	81	61	
3		110	1.8	0.054	2.032	0.0089	81	70	
4		165	1.6	0.051	3.186	0.0061	86	68	
5		—	—	0.038	3.170	0.0026	86	63	
6		—	—	0.046	3.170	0.0040	85	67	
7		—	—	0.044	3.121	0.0023	86	65	
1	2	70	5.5	0.042	0.225	0.0082	78	85	5
2		154	7.0	0.049	0.944	0.0147	140	100	
3		115	2.0	0.050	1.541	0.0062	150	120	
4		241	2.0	0.064	3.170	0.0112	165	170	
5		—	—	0.041	2.993	0.0032	160	140	
6		—	—	0.056	3.005	0.0026	160	130	
7		—	—	0.038	3.030	0.0014	170	150	
1	3	82	6.5	0.043	0.292	0.0029	72	87	10
2		183	8.0	0.046	1.231	0.0131	190	110	
3		136	2.5	0.050	2.008	0.0070	200	100	
4		206	2.5	0.043	3.206	0.0118	205	110	
5		—	—	0.046	3.192	0.0047	225	120	
6		—	—	0.045	3.135	0.0041	215	110	
7		—	—	0.055	3.066	0.0055	210	140	

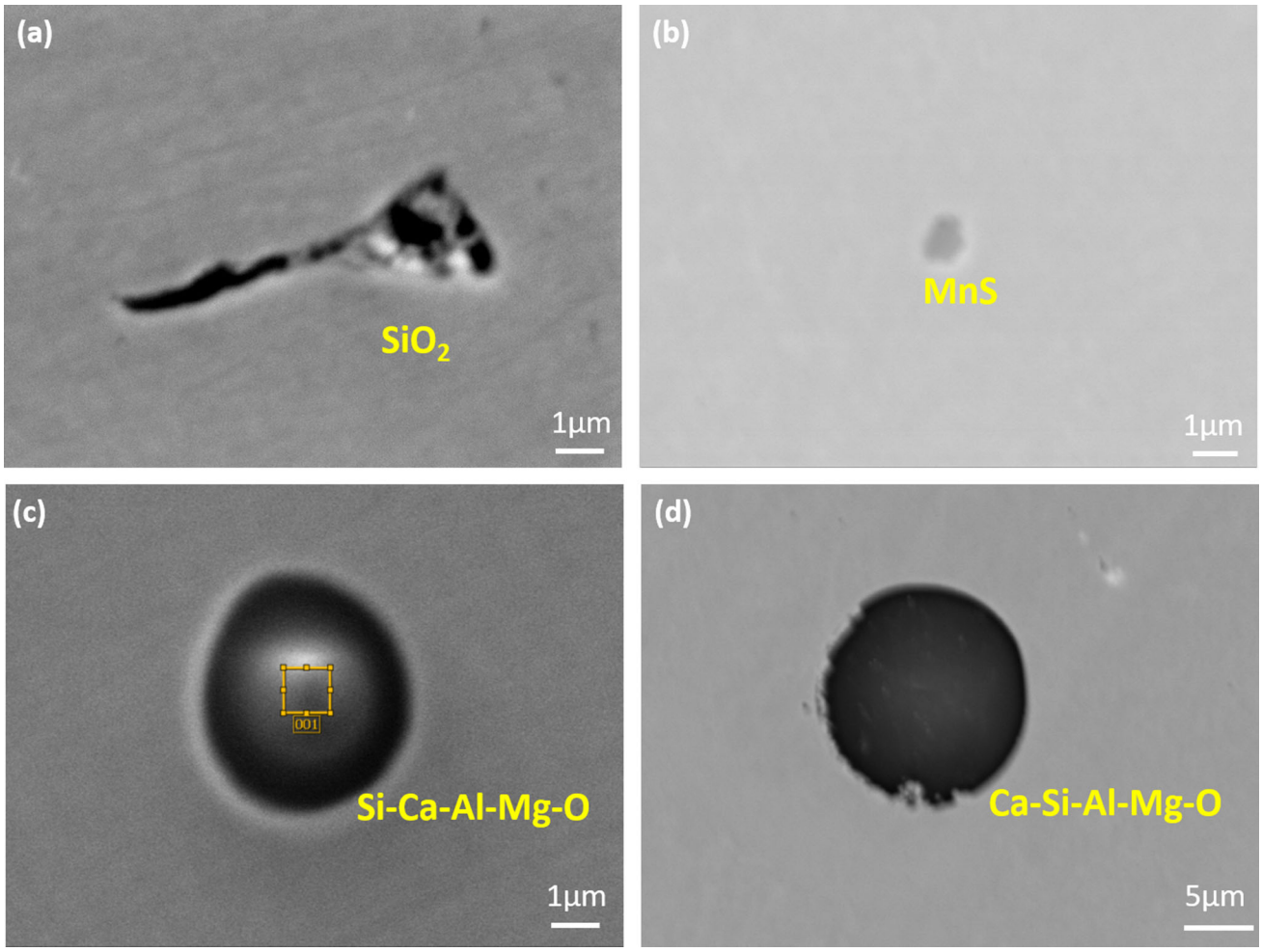

Fig. 5—SEM micrographs of NMIs in the steel treated with synthetic slag without the addition of SCO; (*a*) SiO_2 deoxidation product; (*b*) MnS inclusion; (*c*) complex oxide inclusion; (*d*) complex oxide with MnS ring.

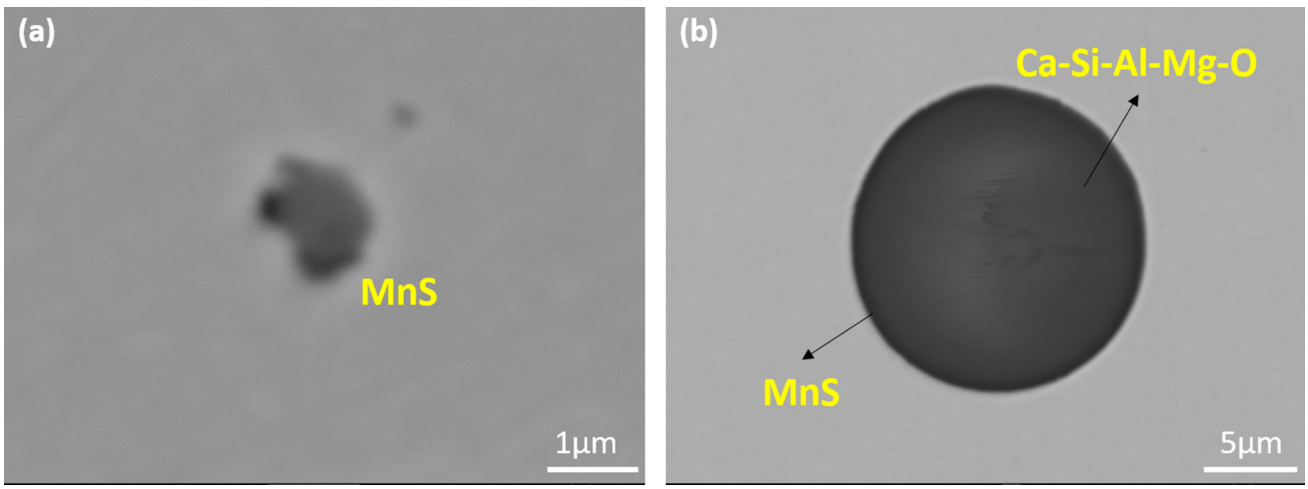

Fig. 6—SEM micrographs of NMIs in the steel treated with synthetic slag and 5 kg/t of SCO; (*a*) MnS inclusion; (*b*) complex oxide with MnS ring.

interesting to note that the inclusion is rich in sulfur concentration; however, it is deficient in manganese content. Therefore, it can be summarized that the complex oxide inclusion evolved to Mn free oxy-sulfide inclusion in the high Si electrical steel when the top slag is contaminated with an excess amount of SCO.

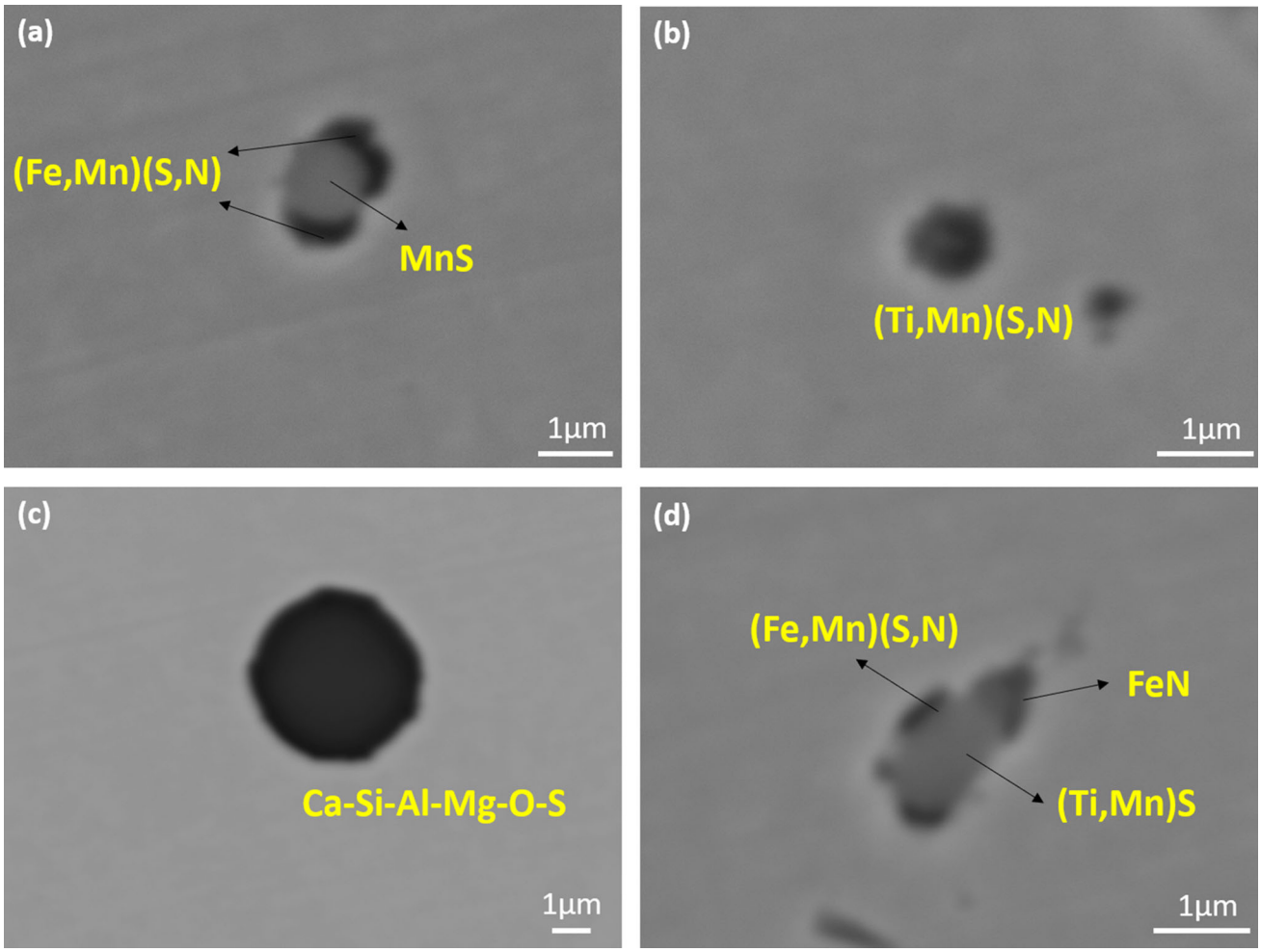

Fig. 7—SEM micrographs of NMIs in the steel treated with synthetic slag and 10 kg/t of SCO; (*a*) and (*b*) co-precipitated nitride and MnS inclusion, (*c*) oxy-sulfide inclusion, and (*d*) complex sulfide with iron nitride inclusion.

4. *Magnetic properties*

The strong microstructure-magnetic correlations in Fe-Si soft magnetic alloys allowed us to study the magnetic properties concerning different inclusion characteristics of the steel samples. Figures 10(a) and (b) represent the saturation magnetization curve for all the Heat obtained from the magnetometry and electromagnetic surface probe technique, respectively. It is observed from the figure that all the samples exhibit ferromagnetic behavior identified by a small area under the loop of the saturation magnetization curve. Figure 10(a) inset shows a comparable saturation magnetization (M_s) for all the Heat representing compositional homogeneity among the three samples. In addition, the M–H curves obtained from the electromagnetic sensor probe technique, while scanning the large sample volume, depict poor magnetic characteristics of the Heat 3 samples concerning the magnetic flux density and coercivity, as shown in Figure 11 (also refer to Figure 10(b)). Also, the Heat 3 sample shows relatively poor permeability compared to the other samples, as seen in Figures 10(a) and (b), confirming the poor soft-magnetic characteristics of the sample. Based on the magnetic properties obtained from both techniques, it can be confirmed that the high silicon steel treated with synthetic slag, lime, and 10 kg/t of SCO exhibits poor magnetic behavior compared to the other studied samples.

IV. DISCUSSION

A. *Thermodynamic Analysis of Inclusion Evolution*

The present investigation deals with the top slag treatment of high Si electrical steel using lime-rich high basicity synthetic slag. The experiments conducted in this investigation are evaluated for the slag path in the relevant pseudo ternary diagram constructed at 1600 °C using FactSage 6.4, a commercial thermodynamic simulation software package. Figure 12 demonstrates that the composition of slag changes from a lime-rich high basicity region to a low basicity region in the CaO-SiO_2-Al_2O_3 pseudo ternary diagram due to the assimilation of silica-rich deoxidation products in the top slag during alloying and refining of high silicon steel. The slag path followed for experiments conducted without SCO is shorter (AB) than the experiments conducted

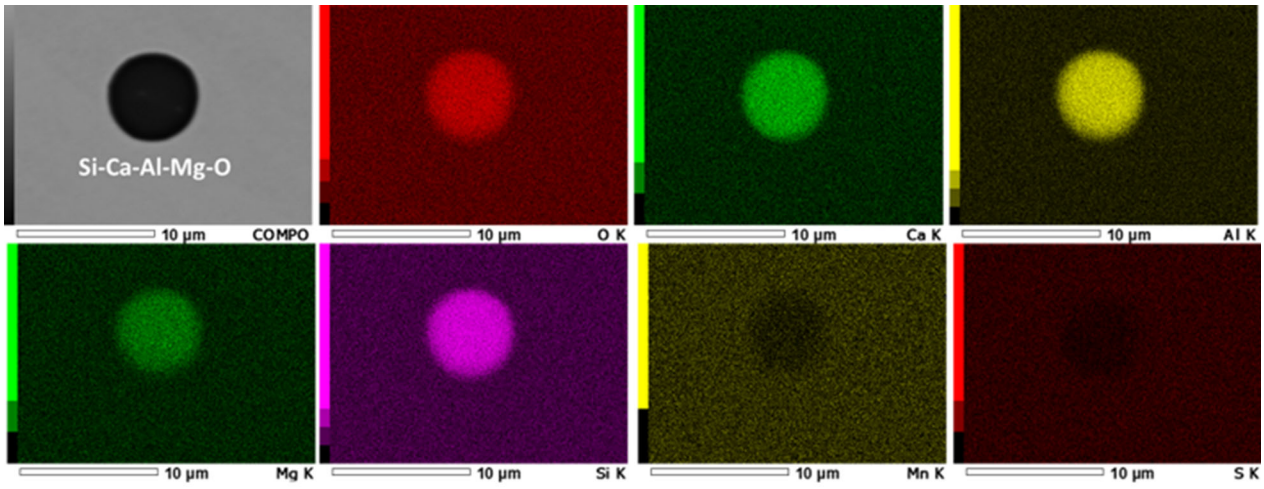

(a)

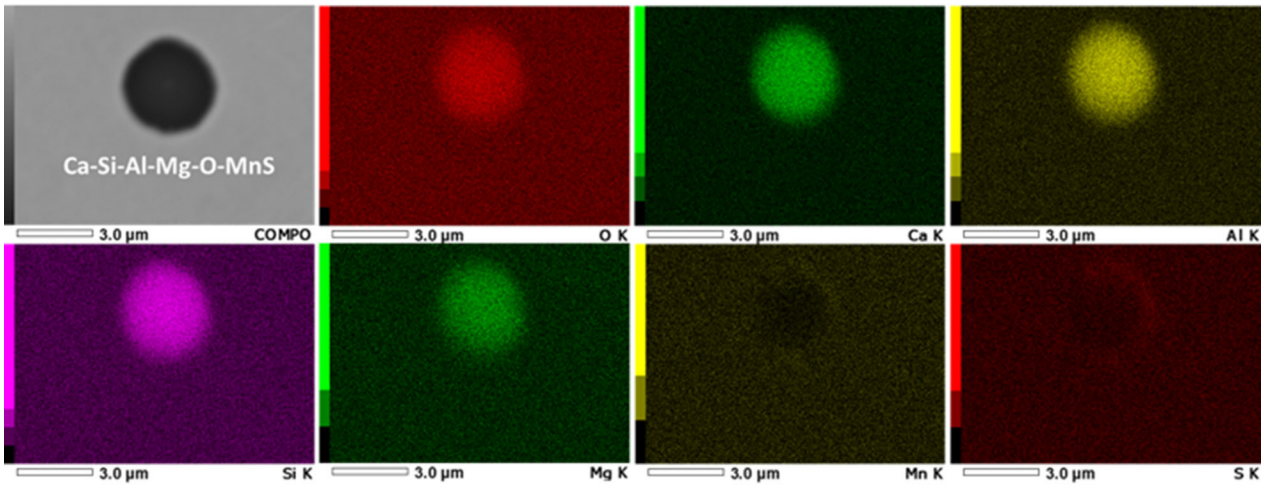

(b)

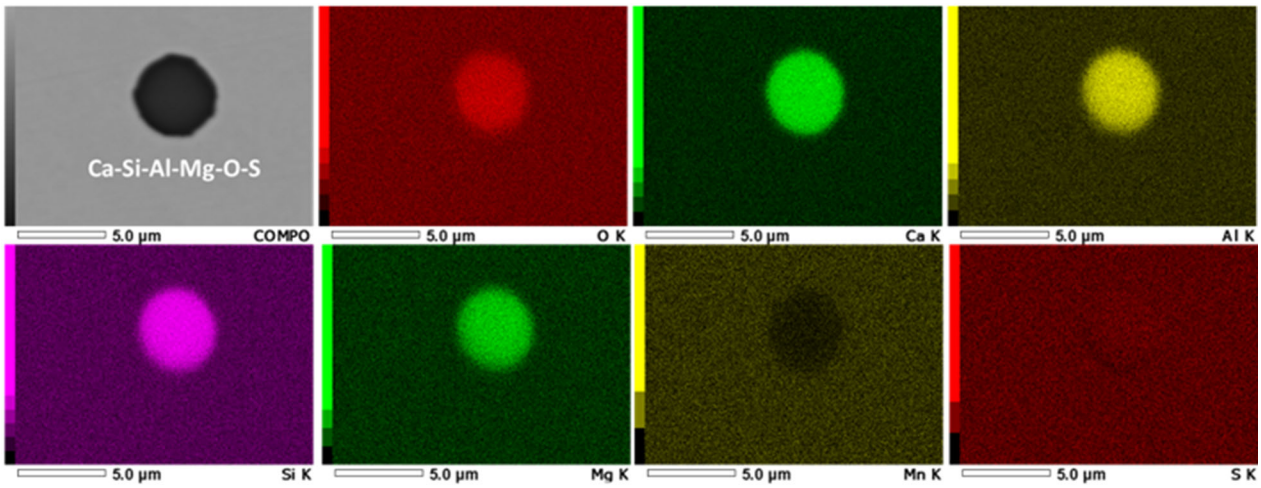

(c)

Fig. 8—EDS elemental mapping of calcium-based (*a*) complex oxide inclusion in Heat 1, (*b*) oxide core and MnS ring-type inclusion in Heat 2, and (*c*) oxy-sulfide inclusion in Heat 3.

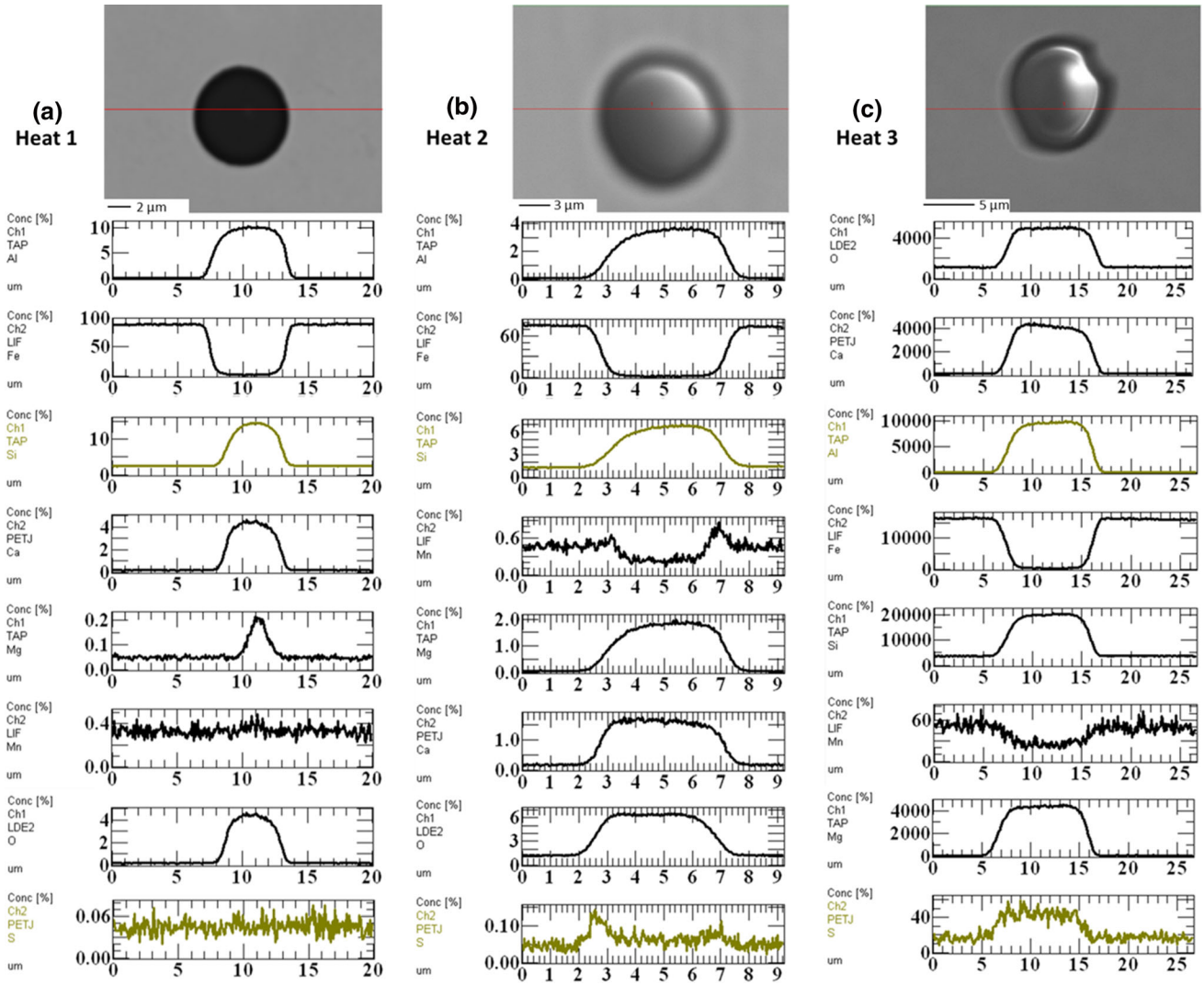

Fig. 9—EPMA-WDS line scan analysis of complex oxide inclusions in the steel refined with contaminated top slag (*a*) Heat 1: 0 kg/t, (*b*) Heat 2: 5 kg/t, and (*c*) Heat 3: 10 kg/t of SCO.

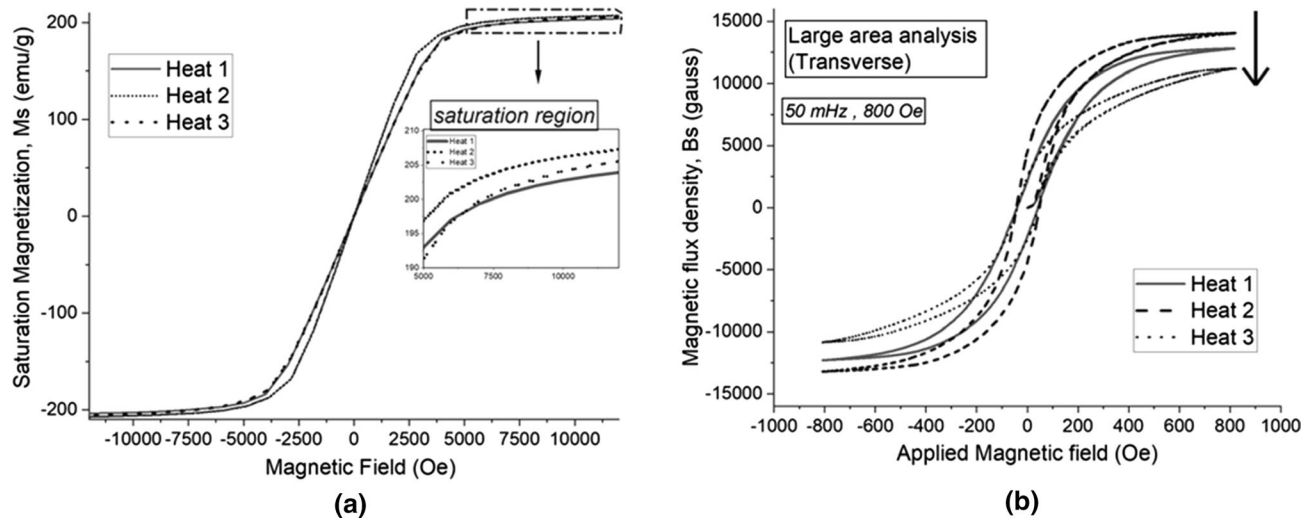

Fig. 10—Saturation magnetization curves (M–H) obtained from (*a*) magnetometry and (*b*) electromagnetic surface probe for the steel samples.

with SCO (ACB), as shown in the pseudo ternary diagram. It is mainly attributed to the reaction between reducible oxides in slag and deoxidizers.[27,28] Consequently, the change in slag path due to contaminated top slag also results in poor desulfurization of the liquid steel (refer Table II).

Further, the evolution of sulfide and oxide inclusions in the high silicon steel has been studied using the equilibrium module of FactSage and represented in Figure 13. Figures 13(a) and (b–d) depict the precipitation of MnS and oxide inclusions during the equilibrium solidification of high silicon steel, respectively. As shown in Figure 13(a), the property diagram demonstrates the early precipitation of MnS in the Heats treated with SCO compared to Heat 1 during solidification. This is primarily due to the higher content of sulfur in steel treated with SCO as a result of poor desulfurization during top slag refining, as explained earlier. The precipitation characteristics of oxide inclusions in all the Heat are similar (refer Figure 13(b) through (d)). The globular oxide inclusions observed in the steel samples are mostly the liquid inclusions present at high temperatures, as confirmed by the property diagrams shown in Figure 13. The transformation of liquid inclusions to other complex oxide inclusions during solidification seems difficult due to supercooling and sluggish diffusion within the complex oxides. Rarely pure deoxidation product (SiO_2) was observed in the samples. Figure 14 illustrates the elemental sulfur (EPMA-EDS elemental analysis) present in the spherical liquid inclusions increases in the steel samples with the addition of SCO. It confirms the influence of SCO on the chemical characteristics of the liquid (complex) oxide inclusions (also refer Figures 8 and 9). This observation could be connected to the change in physicochemical properties of final slag in the Heat conducted with SCO. The basicity of final slags varied in the narrow range for all the Heat, and dissolution of MgO from refractory lining was high for the experiments conducted with 10 kg/t SCO (refer Table I). This observation is in agreement with other recent findings.[30] A high amount of MgO in the slag raises the viscosity and the liquidus temperature by increasing the solid fraction in the slag at steelmaking temperatures.[31] This further decreases the desulfurization ability of the slag. Moreover, the positive interaction parameter between dissolved silicon and sulfur in liquid steel and a strongly reducing atmosphere during the top slag treatment favors desulphurization. However, the condition of the top slag is not kinetically favorable to absorb sulfur from liquid steel. Therefore, the inclusions present in the melt establish a local equilibrium with the liquid steel. Eventually, the complex oxide inclusions absorb the elemental sulfur and transform into oxy-sulfide inclusions in high Si steel. To summarize, a higher amount of SCO transforms the complex oxide inclusions into sulfur-rich complex oxide (oxy-sulfide) inclusions in

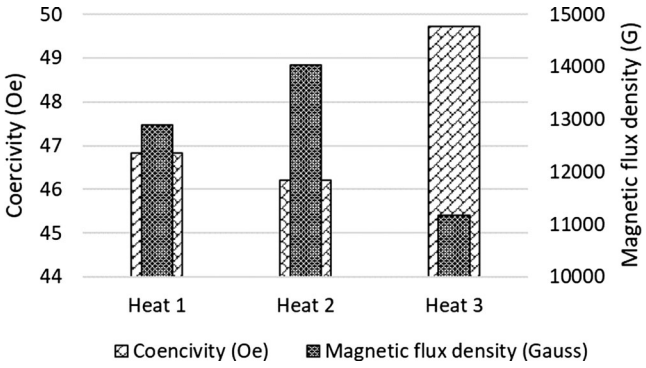

Fig. 11—Comparison of magnetic properties in all the Heats.

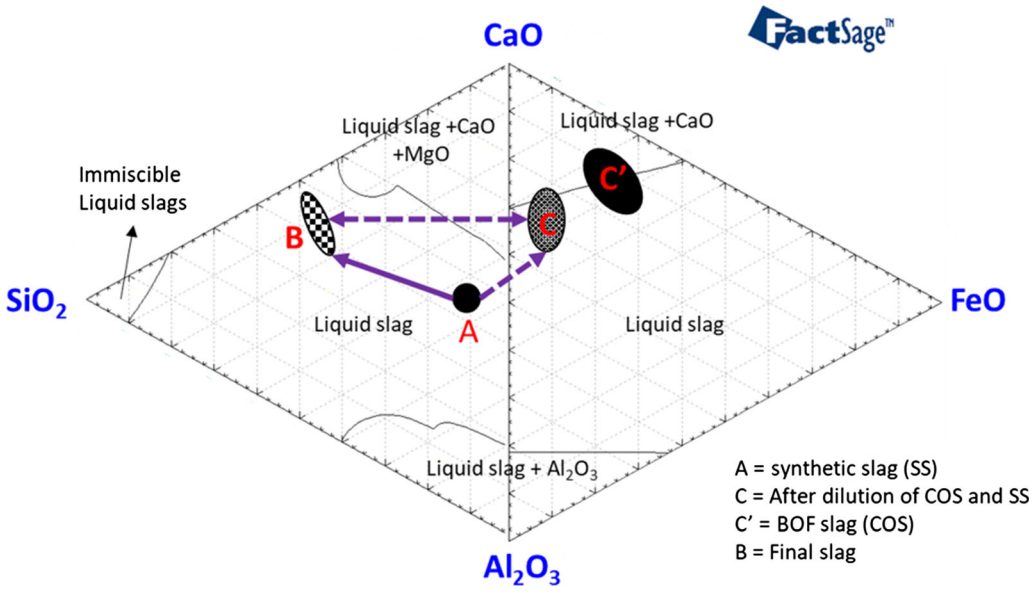

Fig. 12—Schematic representation of slag path in pseudo-ternary diagrams of CaO-SiO_2-Al_2O_3-8 pct MgO and CaO-Al_2O_3-FeO-5 pct MgO-15 pct SiO_2-1.5 pct MnO constructed at 1600 °C.

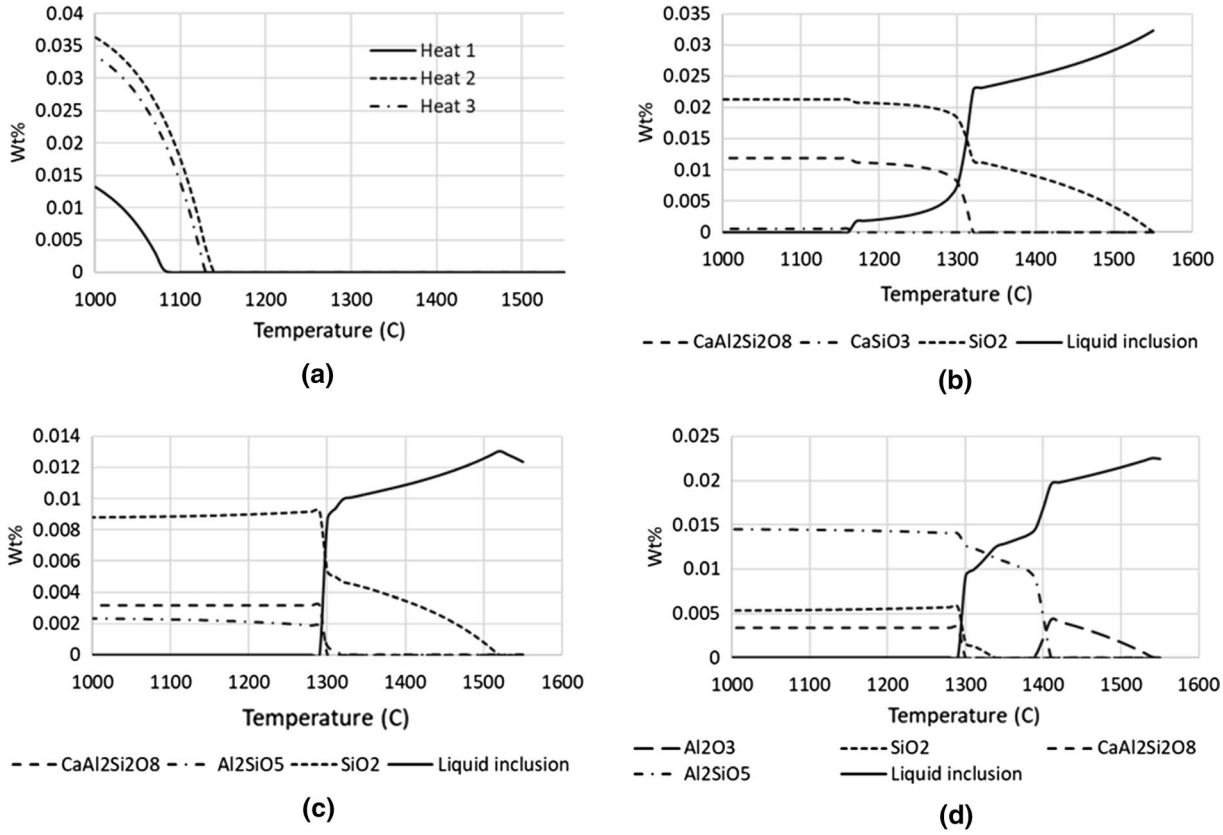

Fig. 13—Evolution of (*a*) sulfide inclusion in all the Heats and (*b*) through (*d*) oxide inclusions during solidification of the liquid steel refined by top slag contaminated (b) without, (c) 5 kg/t and (d) 10 kg/t of SCO.

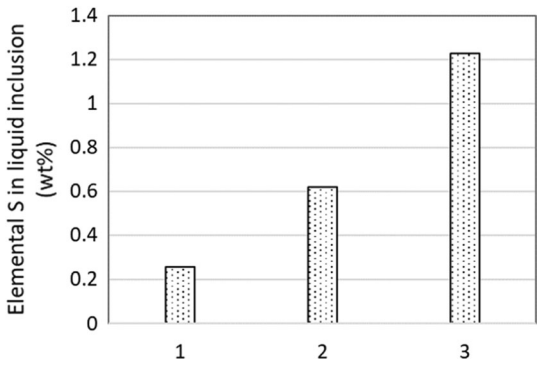

Fig. 14—EPMA determined elemental sulfur in the liquid oxide inclusion after top slag treatment with varying amounts of SCO (Heat 1: 0 kg/t, Heat 2: 5 kg/t, and Heat 3: 10 kg/t).

the high Si steel. The subsequent section will discuss the ill effects of oxy-sulfide inclusions in light of high-grade electrical steel production.

1. *Inclusion-domain wall interaction*

In general, the soft magnetic properties of the material are influenced by intrinsic (chemical composition) and extrinsic (such as size and fraction of phases and precipitates/inclusions, grain size and boundaries, strain fields, bulk texture, *etc.*) properties. Being an intrinsic property of a magnetic material, magnetic flux density (B_s) of soft magnetic material depends on chemical composition and the net volume fraction of the magnetic phase in the specimen. The sharp decline of B_s for Heat 3 compared to other Heat suggests a significant reduction in the magnetic ferrite phase fraction or ferromagnetic dilution by the presence of non-magnetic particles (refer Figure 11). Further, magnetic coercivity (H_c) is a microstructure sensitive property, wherein any presence of non-magnetic matrix phase, grain size, precipitates, strain fields, *etc.*, impacts the soft-magnetic behavior. At a microscopic level, the domain wall movement during the magnetization process is inhibited due to discontinuities like grain boundary, precipitates, and NMIs and increases H_c.[18–25] To confirm SCO's direct and indirect role on inclusions and magnetic behavior, respectively, macro-hardness and grain size of the specimens were compared in this investigation (refer Figure 15). The insignificant variation of average micro-hardness and grain size values of the studied steel samples allow us to neglect the contribution from grain size. Furthermore, the specimens were annealed to eliminate the strain fields that arise during the hot deformation and taken for magnetic characterization. It ensures the negligible interference of magneto-elastic anisotropy during the magnetization process. The deterioration in magnetic properties in Heat 3 (refer Figure 11) despite the uniform

microstructure and strain field in all the samples point toward the excess SCO (10 kg/t) condition and the observed inclusion characteristics (size and number density).

To understand the coercivity loss in Heat 3, the distribution of non-metallic inclusions in the matrix is investigated in detail using the AztecSteel cleanliness assessment tool attached with SEM-EDS. It is evident from Figure 16 that the number density of sub-micron size inclusions increases with an increase in the amount of SCO in the top slag. Though the number density of inclusions is high in Heat 2 compared to Heat 1, the magnetic behavior is similar. This might be due to the presence of inclusions in size and number density, which are inefficient to pin the domain walls, as confirmed by other researchers.[23,25] Specifically, a few studies[23,25] relate the compositional sensitivity of inclusions to their morphology and size distribution. The present work outlines the distribution of sub-micron to micron-sized compositionally different complex inclusions and corresponding variation in the magnetic coercivity. The coercivity (H_c) exhibits maximum sensitivity to the precipitates/inclusions present inside the grain rather than grain boundaries.[32] Similarly, the different compositional arrangements comprising oxy-sulfide precipitate in Heat 3 samples might contribute to the sub-micron precipitate size and spatial distribution (inter-particle spacing) inside the grain. The aforementioned microstructural characteristics contribute to the effective domain wall pinning and increase the coercivity (H_c) of Heat 3 samples. In support of our argument, the voltage signal (V_{sensor}) of the current MagStar device is proportional to the number of pinning and un-pinning events during the magnetization process (dM/dt).[23,33,34]

2. *Industry implication of present findings*

One of the important aspects of electrical steel is to control the size, shape, and distribution of sulfide inclusions to preserve the Goss nuclei and assist the abnormal Goss grain growth during the later stage of secondary recrystallization.[17] It is to be noted that systematic research related to the influence of SCO on the refining practice and evolution of non-metallic inclusion in high silicon electrical steel is scanty. The present investigation throws light on inclusion evolution due to SCO during top slag refining of high silicon steel. It can be well submitted that the production of high-grade cold rolled grain oriented (CRGO) silicon steel is a confidential technology in any steel plant. Only a few steel makers successfully produce high-grade silicon steel for functional applications due to the complexity involved in the Goss texture evolution. The general downstream operations in the silicon steel production process are schematically represented in Figure 17. The important aspects of NMIs in the relevant stages are also indicated in the figure.

In general, it is essential to utilize the NMIs (mostly sulfides and nitrides) efficiently to control the growth process of Goss grains during the annealing stages.[35–37] The primary function of sulfide inclusions to promote Goss texture during the annealing process and reduce the core loss in the steel sheet is,[38–42]

- Inhibition of the Goss oriented nuclei growth during primary recrystallization (PRx) annealing
- Selective dissolution of MnS inclusions during secondary recrystallization (SRx) annealing to allow abnormal grain growth of preserved Goss oriented nuclei during secondary recrystallization (SRx) annealing
- Eventually, the removal of sulfur from the matrix to the slurry coated oxide layer in the steel sheet

It should be noted that decarburization of the steel sheets also occurs during the SRx annealing process. Removal of sulfur from the matrix after recrystallization is essential to reduce further the core loss of the silicon steel.[24] To achieve the above functions, the homogeneous distribution of fine sulfide (MnS) inclusions is crucial before the start of the annealing process.[36] The pre-requisite for the homogeneous distribution of fine MnS in the steel product is the complete dissolution of MnS inclusions during the reheating process. The dissolution of MnS in electrical steel strongly depends on the Mn/S ratio, temperature, and size.[43] The modern steelmaking practice (i.e., thin slab casting direct rolling) involves the integration of the continuous casting and reheating process to reduce energy consumption without compromising the product quality. This innovation further calls for lowering the temperature and holding time in the reheating furnace. Therefore, engineering MnS inclusions to dissolve at

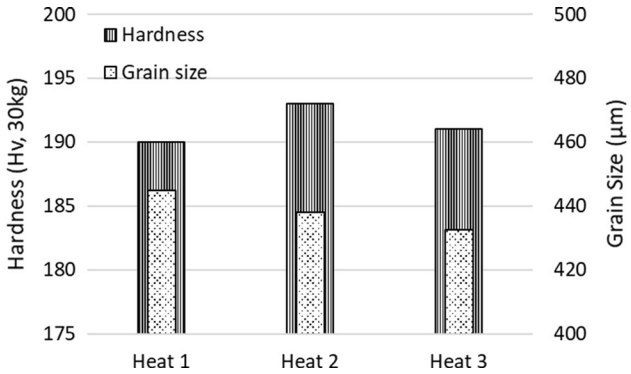

Fig. 15—Comparison of hardness and grain size is all the Heats.

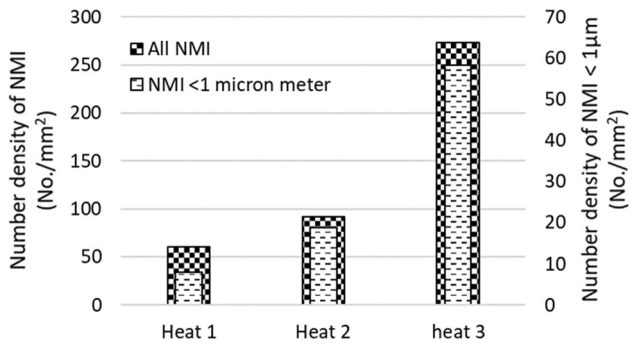

Fig. 16—Comparison of the number density of NMI is all the Heats.

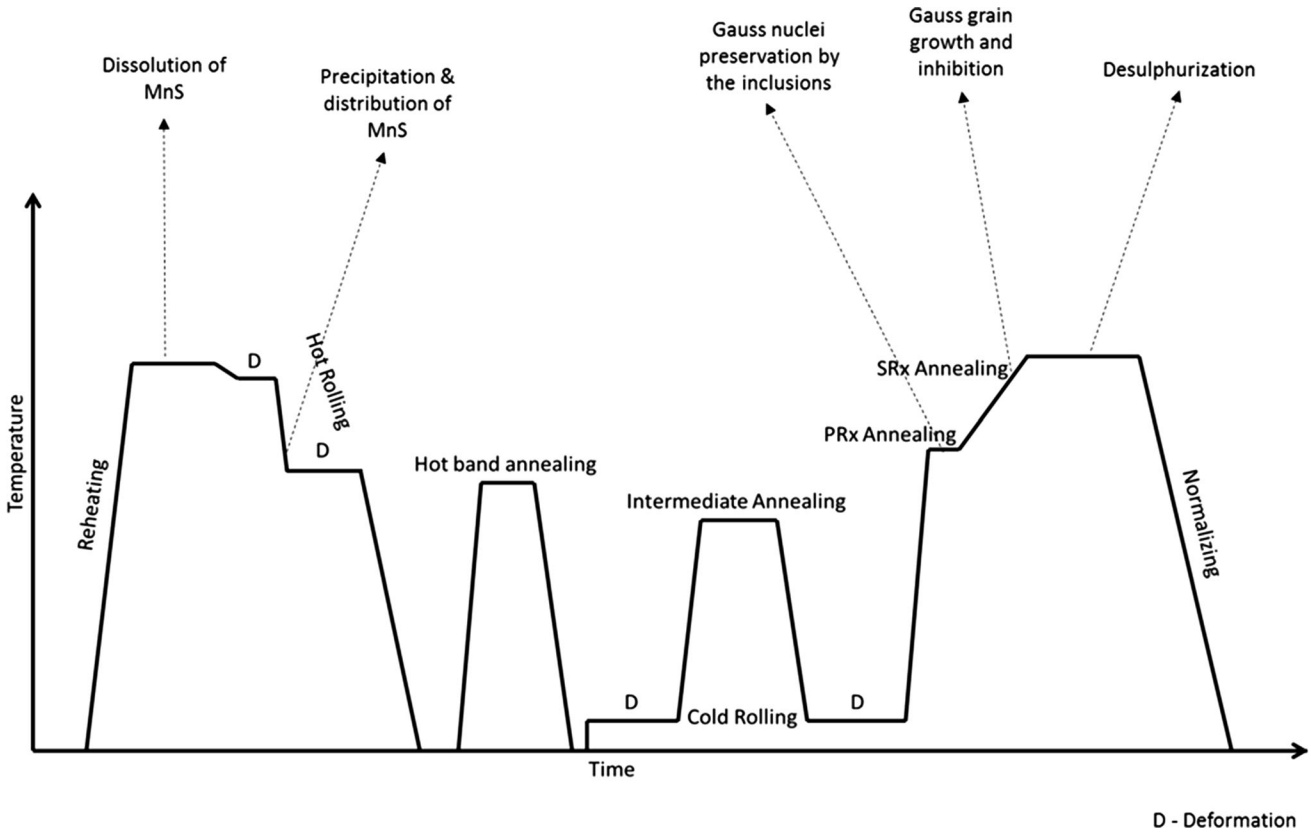

Fig. 17—Downstream processes involved in the production of high Si electrical steel.

low reheating temperatures is one of the major challenges for the economical production of high silicon electrical steel.[44]

The findings of the present investigation apply to the electrical steel manufacturing technology that deals with sulfide inclusions as a Goss grain growth inhibitor. In general, high silicon steel contains less manganese; therefore, the sulfur level in the liquid steel must be controlled in a narrow range to bring out the maximum benefit of using MnS as a grain growth inhibitor. Many investigators reported[7,8] that the desulfurization efficiency of the ladle furnace slag degrades due to the carryover of furnace slag into the ladle. This observation corroborates well with the present findings (refer Table II). Furthermore, the limited information available on SCO's influence on inclusions' chemical characteristics in electrical steel. Other than sulfide inclusions, the residual oxide inclusions in the steel matrix are difficult to remove during downstream operations of high silicon steel, unlike sulfur and carbon. It is noted that removing oxide inclusions during liquid steel treatment is essential to decrease the non-magnetic proportions in the ferromagnetic (steel) matrix and increase the magnetic saturation of the electrical component. Furthermore, it is always preferred to achieve the total oxygen content as low as possible to produce clean steel.

Apart from the number and distribution of inclusions, the composition of inclusions plays a vital role in controlling the functional behavior of the high silicon steel.[45] The complex oxide inclusions present in the high silicon steel, treated only with the synthetic slag, generally consist of Al_2O_3, SiO_2, CaO, and MgO. The sulfide inclusions are precipitated as pure MnS in the steel matrix at a relatively low temperature (refer Figure 13), which can be easily dissolved during reheating process. In the case of the experiment conducted with 5 kg/t of SCO, it is observed that MnS rings surround the complex oxides. However, for the experiment conducted with 10 kg/t of SCO, the inclusions are completely converted to oxy-sulfide type, apart from the pure MnS inclusions (refer Figures 8 and 9). It might be attributed to the fact that the sulfide capacity of the inclusions increases with the increase in SCO, as evident from the present findings (refer Figure 13). It is to be noted that the MnS free oxy-sulfide inclusions are more stable than pure MnS inclusions in the steel matrix. MnS free oxy-sulfide inclusions are expected to form during the refining of high silicon steel. Therefore, the scope for the complete dissolution of sulfide (oxy-sulfide) inclusions is difficult in the normal reheating temperature ranges as practiced in steel industries. It might lead to poor utilization of sulfide inclusions during PRx and SRx processes to maximize the Goss texture evolution. Furthermore, the high stability of oxy-sulfide inclusions is not favorable for removing sulfur from the inclusions to the slurry-coated region during the final annealing process. Consequently, the high fraction of sub-micron size residual oxy-sulfide inclusions in the steel matrix would deteriorate the magnetic behavior of grain-oriented steel.

V. CONCLUSION

This investigation emphasizes precise control of the liquid steel tapping process to produce electrical steel while considering sulfide inclusions as inhibitors for the Goss grain growth in downstream processing. The systematic investigation clarified the role of SCO on inclusion evolution and ensuing magnetic behavior in high silicon steel. The salient findings are,

- Excess SCO (> 5 kg/t) in the top slag reduces its desulphurization ability, inviting the partition of elemental sulfur to the complex oxide inclusions from the liquid steel.
- Due to excess SCO, complex oxide inclusions present in the liquid steel transform into deleterious MnS free oxy-sulfide inclusions.
- Due to contamination of top slag with excess SCO, the number density and distribution of sub-micron size NMIs in the steel matrix increases.
- Magnetic characterization of steel samples reveals that the functional properties deteriorate due to a higher fraction of fine-sized inclusions in the steel matrix.

The envisaged impairments to functional properties of high silicon electrical steel due to excess SCO into the transfer ladle are,

- Inefficient utilization of sulfide inclusion as Goss grain growth inhibitor (leads to decreased Goss texture fraction) during the recrystallization process increases the finished product's core loss.
- The coercively/core loss increases due to the high fraction of fine-sized inclusions that can effectively pin the domain walls during movement.
- The scope for removing oxy-sulfide inclusions at a later processing stage is negligible, unlike the pure MnS. Hence, the magnetic saturation in the finished product decreases due to non-magnetic phases/inclusions.

The understanding developed in this investigation will assist the steelmakers in successfully producing high-quality, high silicon electrical steel.

CONFLICT OF INTEREST

On behalf of all authors, the corresponding author states that there is no conflict of interest.

REFERENCES

1. E. Zinngrebe, P. Seda, C.V. Hoek, and B.V. Arendonk: *ISIJ Int*., 2013, vol. 53, pp. 1913–22.
2. Y. Kurosaki, M. Shiozakl, K. Higashine, and M. Sumimot: *ISIJ Int*., 1999, vol. 39(6), pp. 607–13.
3. D.S. Petrovic, B. Arh, F. Tehovnik, and M. Pirna: *ISIJ Int*., 2011, vol. 51, pp. 2069–75.
4. Y. Luo, A.N. Conejo, L. Zhang, L. Chen, and L. Cheng: *Met. Mater. Trans. B*., 2015, vol. 46, pp. 2348–60.
5. Y. Shinkagi, M. Takashima, T. Nakanishi, and T. Mura: *Grain-Oriented Electromagnetic Steel Sheet and Process for Producing the Same*: Paten No: EP 1 818 420 A1, 2007, JFE Steel Corporation.
6. Z. Liu, J. Wei, and K. Cal: *ISIJ Int*., 2002, vol. 42(9), pp. 958–63.
7. S. He, G. Zhang, and Q. Wang: *ISIJ Int*., 2012, vol. 52, pp. 977–83.
8. Z. Liu, K. Gu, and K. Cal: *ISIJ Int*., 2002, vol. 42(9), pp. 950–57.
9. D. Kaliz: *Arch. Metall. Mater*., 2014, vol. 59(2), pp. 493–500.
10. D. Podorska, and J. Wypartowicz: *Behaviour of Non-Metallic Particles During Solidification of Silicon Steel, Metal*, 2004, p. 1.9.
11. C.K. Hou and C.C. Liao: *ISIJ Int*., 2008, vol. 48(4), pp. 531–39.
12. J.D. Evans, and W.R. Long: *Rare earth metal treated cold rolled, non-oriented silicon steel and method of making it*: Patent No: US 3960616 A, 1976, Armco Steel Corporation.
13. L. Zhang and B.G. Thomas: *ISIJ Inter*., 2003, vol. 43, pp. 271–91.
14. K. Beskow, J. Jia, C.H.P. Lupis, and Du. Sichen: *Ironmak. Steelmak*., 2002, vol. 29, pp. 427–36.
15. K. Steneholm: *The effect of Ladle Vacuum treatment on Inclusion Characteristics for Tool steels*, Doctoral Thesis, KTH Royal Institute of technology, Stockholm, 2005.
16. P. Gardin, J.-F. Domgin, M. Simonnet, and J. Lehmann: *Proceedings of an International Steelmaking Conference*, La Revue de Metallurgie - CIT – Fevrier, 2008, pp. 84–97.
17. A. Honda, Y. Obata and S. Okamura: *History and Development of Non-Oriented Electrical Steel in Kawasaki Steel*, Kawasaki Steel Technical Report, No. 39, 1998.
18. L.J. Dijkstra and C. WERT: *Phys. Rev*., 1950, vol. 79, pp. 979–85.
19. M. Asanuma and S. Miyahara: *J. Faculty Sci*., 1952, vol. 4, pp. 147–52.
20. H.-D. Dietze: *Phys. kondens. Materie*, 1964, vol. 2, pp. 117–32.
21. A.T. English: *J. Appl. Phys*., 1969, vol. 40, pp. 1573–74.
22. T. Ishikawa, Y. Hamada, and K. Ohmori: *IEEE Trans. Magn*., 1989, vol. 25, pp. 3434–36.
23. S. Turner, A. Moses, J. Hall, and K. Jenkins: *J. Appl. Phys*., 2010, vol. 107, p. 09A307-1-3.
24. N. Chukwuchekwa: *Theory of coercive Force for Randomly Distributed Lattice Defects and Precipitations*, Ph.D. Thesis, Cardiff University, 2011.
25. J. Liu, J. Wilson, C.L. Davis, and A. Peyton: *J. Magn. Magn. Mater*., 2019, vol. 481, pp. 55–67.
26. A. Kamaraj, G.K. Mandal, and G.G. Roy: *Met. Mater Trans. B*, 2019, vol. 50B, pp. 438–58.
27. A. Kamaraj, S. Hore, P. Sathyamoorthi, G.G. Roy, and G.K. Mandal: *Trans. Ind. Inst. Met*, 2017, vol. 70, pp. 2465–76.
28. P.C. Pistorius: *J. South Afr. Inst. Min. Metall*., 2019, vol. 119, pp. 557–61.
29. R.K. Roy, A.K. Panda, and A. Mitra: Electromagnetic characterization of steels through magnetic NDE device. *International Conference on Signal Processing and Communication Engineering Systems*, 2015, vol. 2015, pp. 511–14.
30. D. You, C. Bernhard, P. Mayer, J. Fasching, G. Kloesch, R. Rossler, and R. Ammer: *Metall. Trans. B*, 2021, vol. 52B, pp. 1854–65.
31. M. Mohanasundaram, G.G. Roy, and S. Prakash: *Trans. Ind. Inst. Met*, 2019, vol. 72, pp. 1111–18.
32. A. Krishnan, S. Dutta, K. Subramanian, A.K. Panda, P. Murugaiyan, and R.K. Roy: *Trans. Indian Inst. Met*., 2018, vol. 71, pp. 2395–2402.
33. J.N. Mohapatra, T.S. Babu, S.K. Dabbiru, and G. Balachandran: *J. Non Destruct. Eval*., 2021, vol. 40, p. 73.
34. J. Liu, G. Tian, B. Gao, K. Zeng, Q. Liu, and Y. Zheng: *Sensors*, 2021, vol. 21(8310), pp. 1–19.
35. J. Hoon Oh, S.H. Cho, and J.J. Jonas: *ISIJ Int*., 2001, vol. 41(5), pp. 484–91.
36. W. Mao and H. Ren: *Steel. Res. Int*., 2014, vol. 87(12), pp. 1577–82.
37. I. Samajdar, S. Cicale, B. Verlinden, P. Van Houtte, and G. Abbruzzesse: *Scripta Mater*., 1998, vol. 39(8), pp. 1083–88.
38. Z. Zulhan, C. Schrade, and Y.A. Patriona: *Desulfurization of Molten Steel in RH-Degasser by Powder Blowing to Produce Non-Grain Oriented (NGO) Silicon Steel*, SEAISI Conference and Exhibition, Session 6A-6, Pattaya – Thailand, 4th June 2013.
39. D.W. Taylor: *Silicon steel coated with Magnesia containing chromic oxide*, Patent No: US 3,544,396, Armco Steel Corporation, 1970.
40. T.H. Shen: *Metall. Trans. A*, 1986, vol. 17A, pp. 1347–51.
41. S. Szymura, J. Kieszniewski, and A. Zawada: *Mater. Lett*., 1983, vol. 2, pp. 97–100.

42. Y. Hayakawa: *Sci. Technol. Adv. Mater.*, 2017, vol. 18(1), pp. 480–97.
43. K. Iwayama and T. Haratani: *J. Magn. Magn. Mater.*, 1980, vol. 19, pp. 15–17.
44. Y. Liu, X. Zhang, P. Wang, and D. Li: *Metall. Trans. B*, 2020, vol. 51B, pp. 22–26.
45. G. Paltanea, V. Manescu, R. Stefanoiu, I.V. Nemoianu, and H. Gavrila: *Materials (Basel)*, 2020, vol. 20, pp. 1–17.